



Simulation test of spalling failure of surrounding rock in rectangular tunnels with different height-to-width ratios

Feng-qiang Gong^{1,2,3} · Wu-xing Wu¹ · Tian-bin Li²

Received: 4 July 2019 / Accepted: 27 January 2020 / Published online: 6 February 2020
© Springer-Verlag GmbH Germany, part of Springer Nature 2020

Abstract

Spalling (Slabbing) is a typical failure phenomenon, which often occurs after excavation of rectangular tunnel. It has a serious impact on the construction, support and stability of the tunnel. To investigate the characteristics and mechanism of spalling-failure in rectangular tunnel, a series of tests were carried out on granite rectangular tunnel with different height-to-width ratios (H/Ws) (1/2, 3/4, 1/1, 4/3 and 2/1) by using true triaxial system. The whole process of spalling was monitored and recorded by wireless micro camera. According to the test results, the failure mode and failure characteristics of the sidewall spalling were summarized, and the influence of the H/Ws of the rectangular hole on the failure characteristics and stability of the tunnel were discussed in detail. The test results indicate that when the vertical principal stress is the maximum principal stress, the sidewalls of the specimens experience spalling failure. When the spalling occurs, the crack occurs at the shoulder corner of the sidewall and propagates along the axis, resulting in the spalling damage gradually developing from the local area to the whole sidewall along the axis, and forming the thin rock slab parallel to the sidewall. In addition, rectangular tunnels with different H/Ws clearly influence spalling failure. When the height was the same, the degree of spalling damage decreases with the decrease of its width. On the contrary, when the width was the same, the degree of spalling damage does not decrease with the increase in the height. When the height was equal to the width, the damage degree of the tunnel spalling is the largest, which seriously affects the safety of the tunnel. In the case of the same cross-section area of the tunnel, the stability of the tunnel can be improved by selecting the layout mode with the height greater than the width. It is necessary to strengthen the monitoring of the cracks at the shoulder corner of the tunnel, which can reduce the safety risk of the tunnel. These conclusions are helpful to the design of the tunnel, the prevention of spalling and the improvement of the stability of the tunnel.

Keywords Spalling failure · True triaxial test · Rectangular tunnel · Height-to-width ratios (H/Ws)

Introduction

With developments in deep underground engineering, the application of rectangular-section tunnels has become increasingly common. Because of the complex three-dimensional (3D) stress environment of a deep rock mass, the sectional

shape of a rectangular tunnel with different height-to-width ratios (H/Ws) causes different degrees of disaster. A reasonable sectional shape is helpful for improving the stability of a tunnel-surrounding-rock structure and reducing the damage degree of surrounding rock (Cristescu and Paraschiv 1995; Ren et al. 2005). In addition, many on-site engineering examples show that under the condition of deep high stress, the rectangular tunnel experiences an obvious spalling (slabbing) failure, which can bring enormous risks to production safety (Jiang et al. 2017; Hoek and Brown 2018; Hoek et al. 1995; Exadaktylos and Tsoutrelis 1995; Cai and Kaiser 2018; Gong et al. 2019a). For example, Gong et al. (2019a) carried out a study on spalling failure of a rectangular tunnel with a single H/W, which indicated that a deep rectangular tunnel was prone to stress-induced failure under 3D high-stress conditions, creating an approximately parallel maximum shear stress on the sidewall and resulting in obvious

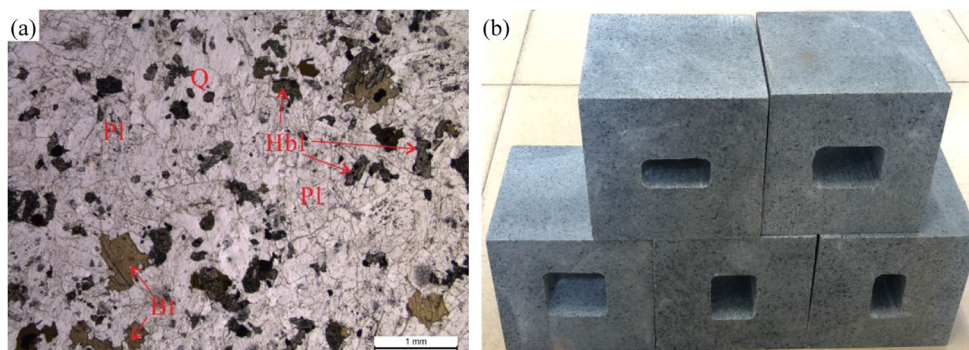
✉ Feng-qiang Gong
fengqiangg@126.com

¹ School of Resources and Safety Engineering, Central South University, Changsha 410083, China

² State Key Laboratory of Geohazard Prevention and Geoenvironment Protection, Chengdu University of Technology, Chengdu 610059, China

³ School of Civil Engineering, Southeast University, Nanjing 211189, China

Fig. 1 The granite specimens: **a** microstructures of granite specimens (Q is quartz, Pl is potassium feldspar, Bt is biotite, Hbl is amphibole) (Gong et al. 2019a); **b** specimens shapes



spalling failure. Therefore, the selection of a reasonable sectional shape, which reduces the occurrence of other rock disasters such as spalling in deep hard-rock tunnels and caverns, has attracted widespread attention from researchers in rock mechanics (Carter 1992; Martin 1993, Martin 1997; Hoek 1965; He et al. 2010, 2012; Zhu et al. 2014; He et al. 2014; Zhou et al. 2016; Du et al. 2016; Li et al. 2018a, b; Gong et al. 2018a, b, 2019a, b; Su et al. 2019).

In the past decades, researchers have carried out a large number of laboratory tests to understand the mechanism of spalling failure of the tunnel sectional shape more fully (Tuncay and Hasancebi 2009; Liang et al. 2016; Du et al. 2019; Gong et al. 2012; Zhao and He 2016; Li et al. 2018a). For example, Du et al. (2019) found that the fracture mode of rectangular and square prism specimens was more likely to change from shear fracture to spalling fracture when the shape ratio was reduced from 3 to 0.5. Li et al. (2018a) conducted a true triaxial unloading test on granite cubic specimens with different H/Ws (between 2.0 and 0.5). It was found that as the H/W of the specimen decreased, a spalling failure was more likely to occur in the case where the intermediate principal stress was low. These experiments were conducted to analyse the influence of different aspect ratios on the spalling of the sidewall (from the perspective of rock-material failure), but the influence of the spatial structure of the section in an actual tunnel on the spalling failure was not considered.

In fact, because of the deep 3D high stress, the damage to the surrounding rocks is affected by the tunnel space structure. Usually, spalling is only a local damage after the tunnel excavation has ended (Li et al. 2012; Xu et al. 2016). For example, after the excavation of Jinping II Hydropower Station, obvious local spalling occurred on the sidewall of the tunnel (Hou et al. 2013; Xu et al. 2016). Therefore, researchers simulated the influence of a spatial structure of a tunnel section on the spalling using rock materials with holes (Carter 1992; Martin 1993, 1997; Hoek 1965; Zhou et al. 2016). Martin (1993, 1997) performed an indoor uniaxial compression test on a circular hole in the Lac du Bonnet granite with a diameter of 5 to 103 mm and observed the spalling failure on the sidewall of the hole. It was also pointed out that when the diameter of the circular hole was larger than approximately 75 mm, the initial stress of the spalling failure was approximately equal to the unconfined compressive strength of granite. Carter (1992) carried out uniaxial compression tests on physical models of nine different hole sizes (diameters between 3.2 and 62 mm) and analysed the effect of size and stress gradient on the spalling of the surrounding rocks. Hoek (1965) and Martin (1993) performed a biaxial compression test on a circular open rock specimen; a failure zone formed by the spalling failure was observed on the sidewall of the hole, and tensile cracks occurred due to spalling failure. Zhou et al. (2016) studied the spalling-failure characteristics of circular holes with different

Fig. 2 Results of uniaxial compression tests on cylindrical specimens (Gong et al. 2019c): **a** typical stress-strain curves, and **b** typical failure characteristics

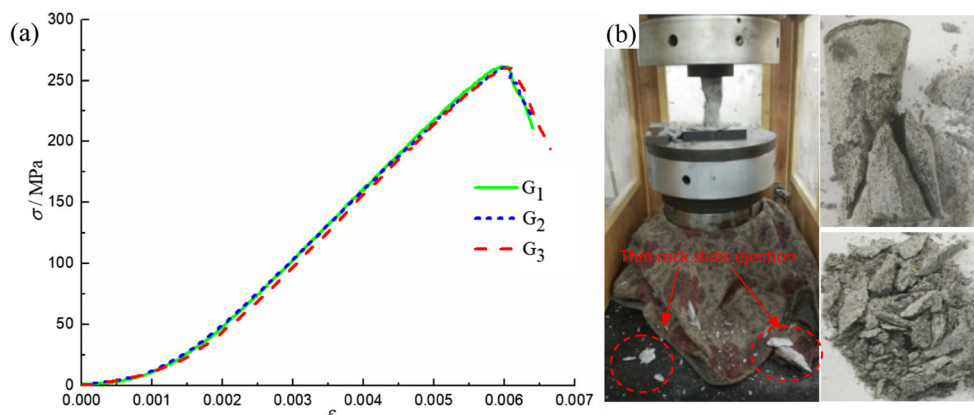


Table 1 Specification of rectangular holes

Specimen no.	Rectangular hole section size (mm)			H/W
	H	W	D	
HW-20-40	20	40	100	1/2
HW-30-40	30	40	100	3/4
HW-40-40	40	40	100	1/1
HW-40-30	40	30	100	4/3
HW-40-20	40	20	100	2/1

bore diameters and straight-wall arch holes with different sizes under a 3D high stress using a true triaxial compression test, then analysed the influence of the radius of curvature of the excavated section on the spalling failure. Martin (1997) drilled a series of vertical boreholes with different diameters of 75, 150, 300, 600 and 1250 mm from the floor of room 405 in the underground research laboratory to analyse and determine the strength-scale effect of different diameters in the field. These studies mainly focused on the spalling test of a sectional shape of a circular tunnel with different diameters, whereas studies on the spalling test of a sectional shape of a rectangular tunnel with different H/Ws are few. In addition, these experimental studies demonstrated that the failure characteristics of spalling are affected by the cross-sectional shape of the tunnel. Therefore, studying the sidewall spalling of rectangular tunnels with different H/Ws under 3D conditions is necessary.

In the present study, five types of rectangular section shapes with different H/Ws (1/2, 3/4, 1/1, 4/3 and 2/1) are designed,

Table 2 Initial in-situ stress at 1000 m depth

Horizontal principal stress		Vertical principal stress σ_v (MPa)
σ_{h1} (MPa)	σ_{h2} (MPa)	
51.0	34.0	27.0

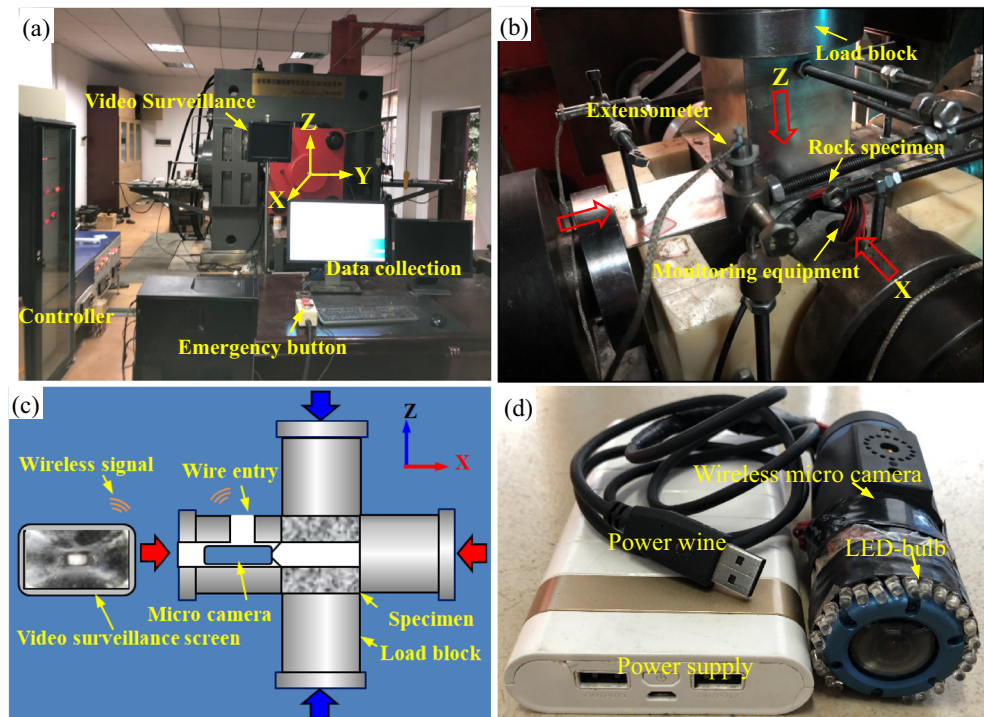
and a series of true triaxial tests are carried out on cubic granite specimens with rectangular holes to study the influence of different H/Ws of rectangular holes on the spalling. In the entire test process, a wireless microcamera is used to monitor and record the whole process of sidewall damage in real time, which can correspond to the 3D stress in real time. By analysing and summarising the spalling-failure process and the rectangular holes with different H/Ws, the influence and mechanism of different H/Ws of the rectangular-hole section on the spalling were obtained.

Experimental design

Rock specimen

To study the process and mechanism of spalling failure in deep rectangular tunnels with different H/Ws, the specimens were selected from granite rock with good integrity and texture. The microstructures of the granite specimens were observed using optical microscopy, and their mineral compositions were analysed (Fig. 1a). They had a primary mineral

Fig. 3 Test equipment: **a** trw-3000 true triaxial equipment; **b** 3D loading device; **c** video monitoring work diagram; **d** wireless micro camera



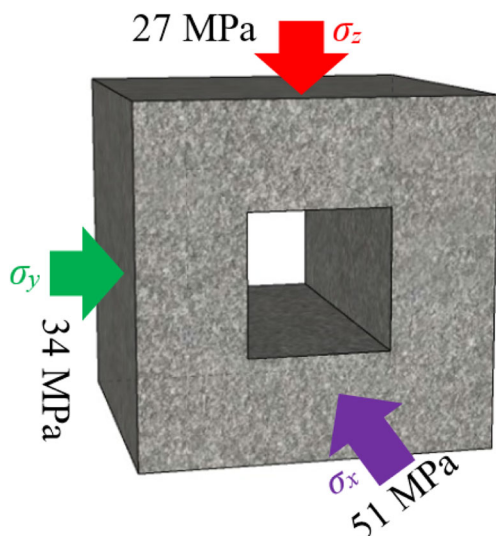


Fig. 4 3D initial stress loading diagram

composition of quartz (~49%; grain size 0.1–0.5 mm), plagioclase (~43%; grain size 0.1×0.4 – 0.4×1.3 mm), biotite (~4%; grain size of 0.04×0.1 – 0.4×0.8 mm), amphibole (~3%; grain size of 0.2–0.8 mm), and apatite and opaque minerals (~1%; grain size of 0.05–0.2 mm). The uniaxial compressive stress-strain curve of the granite specimens are shown in Fig. 2a, and the basic physical and mechanical properties of the granite are obtained. The uniaxial compressive strength, average density and wave velocity of the granite specimens were 261.55 MPa, 2.80 g/cm³ and 5419.00 m/s, respectively. The uniaxial compression failure mode of the granite specimen is shown in Fig. 2b, which shows a sudden brittle failure, and the specimen has a fragment ejection phenomenon, which has a typical rockburst impact tendency (Gong et al. 2019c).

According to existing research results (Gong et al. 2019a), the granite was processed into cubic blocks of $100 \times 100 \times 100$ mm³, and rectangular holes were cut through the cube blocks. To simulate the failure process of rectangular holes with different H/Ws under the 3D high-stress state, the

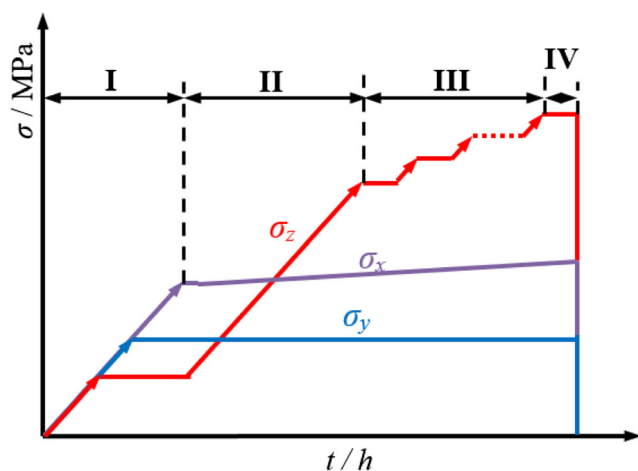


Fig. 5 3D stress path loading schematic

rectangular holes were designed according to the list in Table 1. The prepared specimens are shown in Fig. 1b.

Test equipment

The test was carried using a TRW-3000 rock true triaxial electro-hydraulic servo mutagenesis test machine with a vertical loading capacity of 3000 KN and a horizontal loading capacity of 2000 KN, as shown in Figs. 3a and b. In addition, to observe the process of real-time damage of the rectangular holes under 3D loading conditions, a video surveillance system was installed, as shown in Figs. 3c and d. For the detailed parameters of the experimental equipment, the readers are referred to Gong et al. (2018a).

Three-dimensional stress condition

The failure process of the 3D initial stress environment of the deep rectangular tunnel at the depth of 1000 m was simulated. The calculation method of the 3D initial stress is described in the literature (Gong et al. 2018a), and the calculation results are listed in Table 2. In the test, the rectangular tunnel was arranged along the direction of the maximum initial horizontal direction, and the influence of the surrounding rock stress adjustment on the tunnel sidewall damage was simulated by increasing the Z-direction stress to the maximum principal stress during the test. Therefore, the 3D initial stress of the rectangular hole in the simulation test was $\sigma_x = 51.0$ MPa, $\sigma_y = 34.0$ MPa and $\sigma_z = 27.0$ MPa. The 3D initial stress loading mode is shown in Fig. 4.

Three-dimensional stress loading path

The 3D stress loading path of the specimens in the test is shown in Fig. 5. The specific loading method is described as follows. (I) Initial stress loading stage: the three directions of the specimen were loaded at the same loading rate (0.1 MPa/s) using the load-displacement control method up to the 3D initial stress level. (II) Stress adjustment stage: the Y-direction stress was kept unchanged, and the X-direction was then adjusted to the displacement-load control mode. The displacement was kept unchanged (simplified as plane strain), and finally increase the Z-direction stress with the original loading rate (0.1 MPa/s). (III) Z-direction grading loading stage: to effectively observe the spalling on the sidewall of the specimen, when an obvious local damage of the sidewall of the specimen was observed, the Z-direction stress is adjusted to be graded and kept for a certain period of time. (IV) Unloading stage: when no obvious damage on the sidewall occurred, to prevent overall instability of the specimen, the Z-direction stress loading was stopped and maintain loading for a certain period of time, and finally stop loading in the three directions. The unloading process in this study is described as

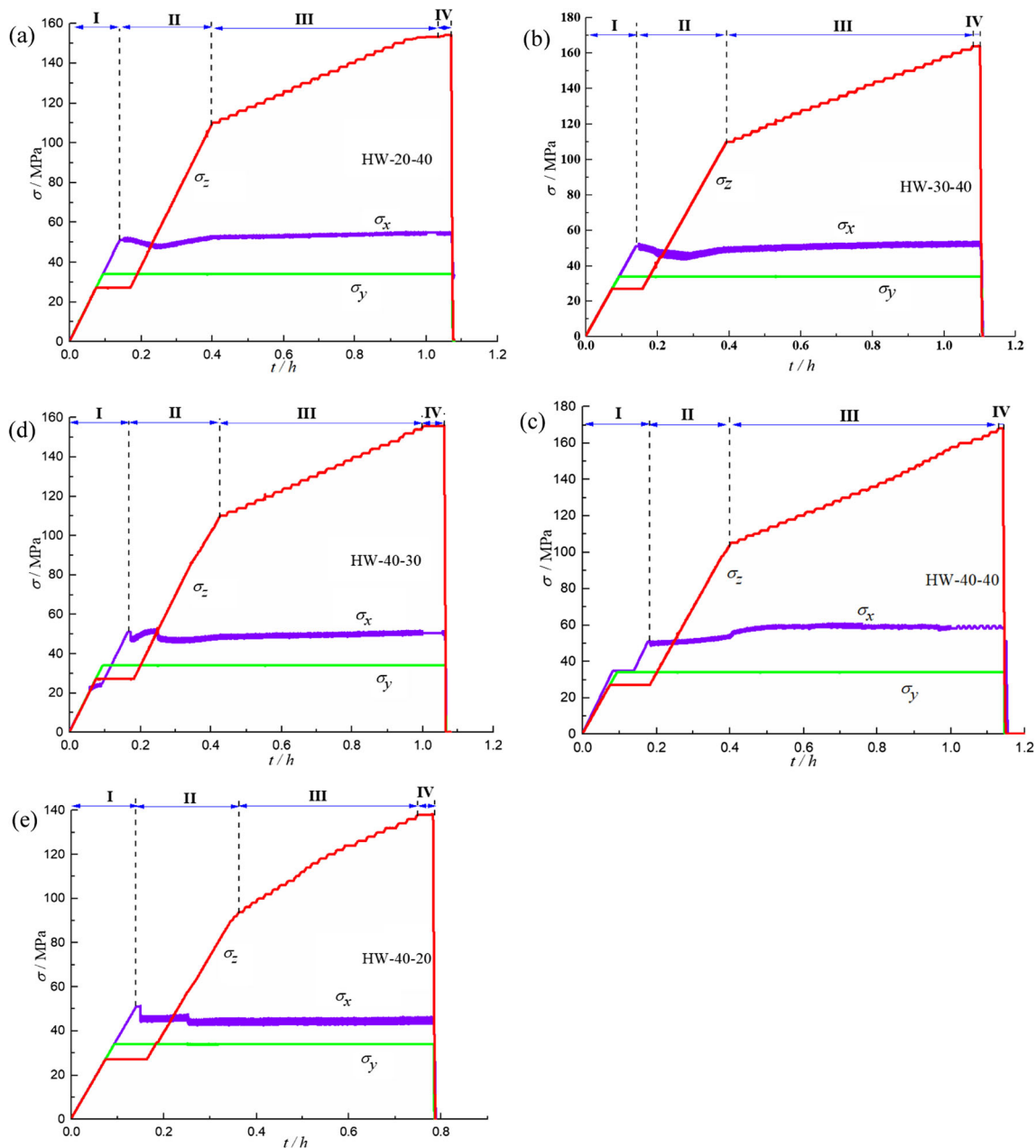


Fig. 6 The actual 3D stress loading diagram of rectangular hole: **a** HW-20-40; **b** HW-30-40; **c** HW-40-40 (Gong et al. 2019a); **d** HW-40-30; **e** HW-40-20

follows. First, σ_z was unloaded to σ_x . Then, they were unloaded together to σ_y . Finally, they were all unloaded to zero.

Experimental results and discussion

Test curve

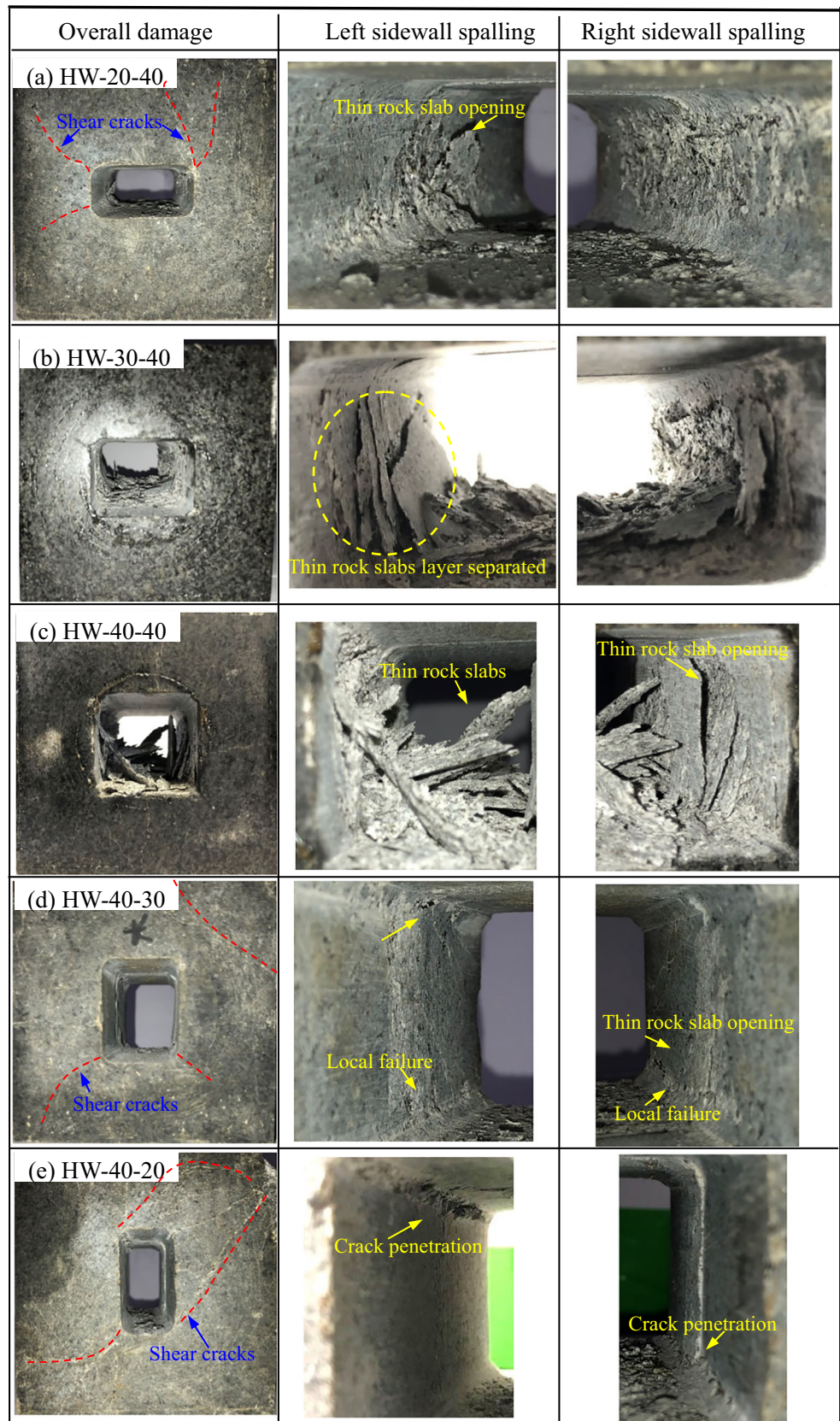
The 3D stress path curve of rectangular holes with different H/Ws after the end of the entire test is shown in Fig. 6. Figure 6 shows that after all the specimens were loaded to the initial

stress level, the X -direction control mode was adjusted from the loading to displacement control, and the X -direction deformation was kept unchanged (i.e. simulating a plane strain problem). With the increase in σ_z , σ_x fluctuated and slowly increased with the increase in σ_z , which was influenced by the Poisson effect and accuracy of the true triaxial-test equipment.

Failure mode of the sidewall

The overall and local failures of the left and right sidewalls in the rectangular holes after the test are shown in Fig. 7, which show that under 3D high-stress conditions, cracks were

Fig. 7 The failure of the whole specimen and the left and right sidewalls after the test: **a** HW-20-40; **b** HW-30-40; **c** HW-40-40; **d** HW-40-30; **e** HW-40-20



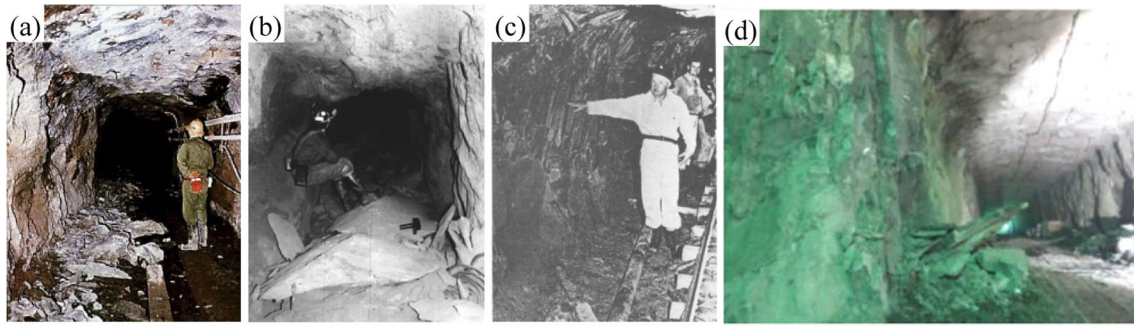


Fig. 8 Examples of on-site spalling: **a** mine tunnel sidewall spalling failure (Hoek and Brown 2018); **b** under high stress right sidewall spalling failure (Hoek et al. 1995); **c** in the transport sidewall spalling (Stacey 1981); **d** sidewall spalling failure (Jiang et al. 2017)

generated on the specimen surfaces, but all specimens remained intact. Significant spalling failure occurred on the sidewalls of all specimens, and the spalling degree was different, because of the different H/Ws of the rectangular holes in the specimens. Some of the sidewalls of the specimens formed obvious thin rock slabs, whereas others exhibited obvious failure zones after the cracks penetrated. Figures 7a–d show that significant spalling failure occurred on the sidewalls, forming thin rock slabs that were approximately parallel to the sidewall. Some thin rock slabs were partially opened due to the cracks that did not completely penetrate, and they were not completely separated from the sidewalls (Figs. 7a and d). Additionally, some thin rock slabs accumulated on the sidewall or fell off to the bottom of the holes, because cracks penetrated through the sidewall (Figs. 7a–c). However, because of the H/Ws of the specimens, no obvious thin rock slabs were generated on the sidewall, and failure zones after the crack penetration were observed only at the shoulder angle of the sidewall (Fig. 7e). Moreover, HW-40-20 exhibited shear cracks that spread from the shoulder angle to the surface of the specimen, especially at the right lower shoulder angle, which indicated that the specimen is prone to overall shear failure (Fig. 7e).

To compare the spalling phenomena in deep tunnels, Fig. 8 shows the typical spalling in the surrounding rock of a deep engineering site. Figures 8a–d show obvious spalling failure of the tunnel sidewall due to the redistribution of the surrounding rock stress after excavation of the deep tunnel. Compared with those shown in Figs. 7 and 8, the failure modes of the sidewalls in the rectangular holes in the test were consistent with those of the in situ rectangular tunnels, demonstrating typical spalling characteristics. This result indicates that the spalling simulation test in this study is reliable for simulating the spalling-failure process of rectangular holes under a 3D stress.

Analysis of spalling-failure process

To understand the specific process of spalling of the sidewall in the rectangular hole in detail, the entire test process

was recorded using a wireless miniature camera, and the typical damage image of the sidewall of the hole was recorded by video to illustrate the spalling-failure process, as shown in Fig. 9. Obvious spalling failure occurred on the sidewalls in the rectangular holes, and some thin rock slabs fell off. Owing to the different H/Ws of each specimen, the degree of spalling on the sidewalls was also different. However, the failure modes of all specimens were the same, which indicated that the typical tensile failure and spalling-failure processes on the sidewall were the same. Therefore, by considering the spalling-failure process of the HW-20-40 specimen as an example, the spalling-failure process was analysed in detail as follows (Fig. 9a): When loaded at the 3D initial-stress level, the sidewall of the specimen was not damaged (Fig. 9a₁). When σ_z was increased to 52.1 MPa, microcracks were generated at the upper and lower shoulders of the sidewall (Fig. 9a₂). With the increase in σ_z , the crack propagated along the lower shoulder angle on the left sidewall and upper shoulder angle on the right sidewall, accompanied by ejection of fine particles during the crack propagation (Fig. 9a₃). Next, the crack continuously propagated along the axis at the shoulder angles on both sidewalls (Figs. 9a₄–a₆). When $\sigma_z = 144.0$ MPa, the cracks partially penetrated the shoulder angles of the left and right sidewalls, resulting in a large quantity of fine particles falling off (Fig. 9a₇). As σ_z increased to 148.0 MPa, thin rock slabs parallel to the maximum vertical principal stress were formed on the right sidewall and opened, which was an obvious indication of a spalling failure (Fig. 9a₈). When $\sigma_z = 152.3$ MPa, the initial thin rock slab on the right sidewall finally fell off to the bottom of the hole, and cracks continued to propagate and partially penetrated, resulting in a new thin rock slab on the right sidewall. Meanwhile, the thin rock slab formed on the left sidewall remained in an open state (Fig. 9a₉). When σ_z increased to 153.8 MPa, the thin rock slabs on both sidewalls continued to open, and the thin rock slabs on the right sidewalls were more obviously separated (Fig. 9a₁₀). At 154.0 MPa, the thin rock slabs on both sidewalls fell off, and the new thin rock

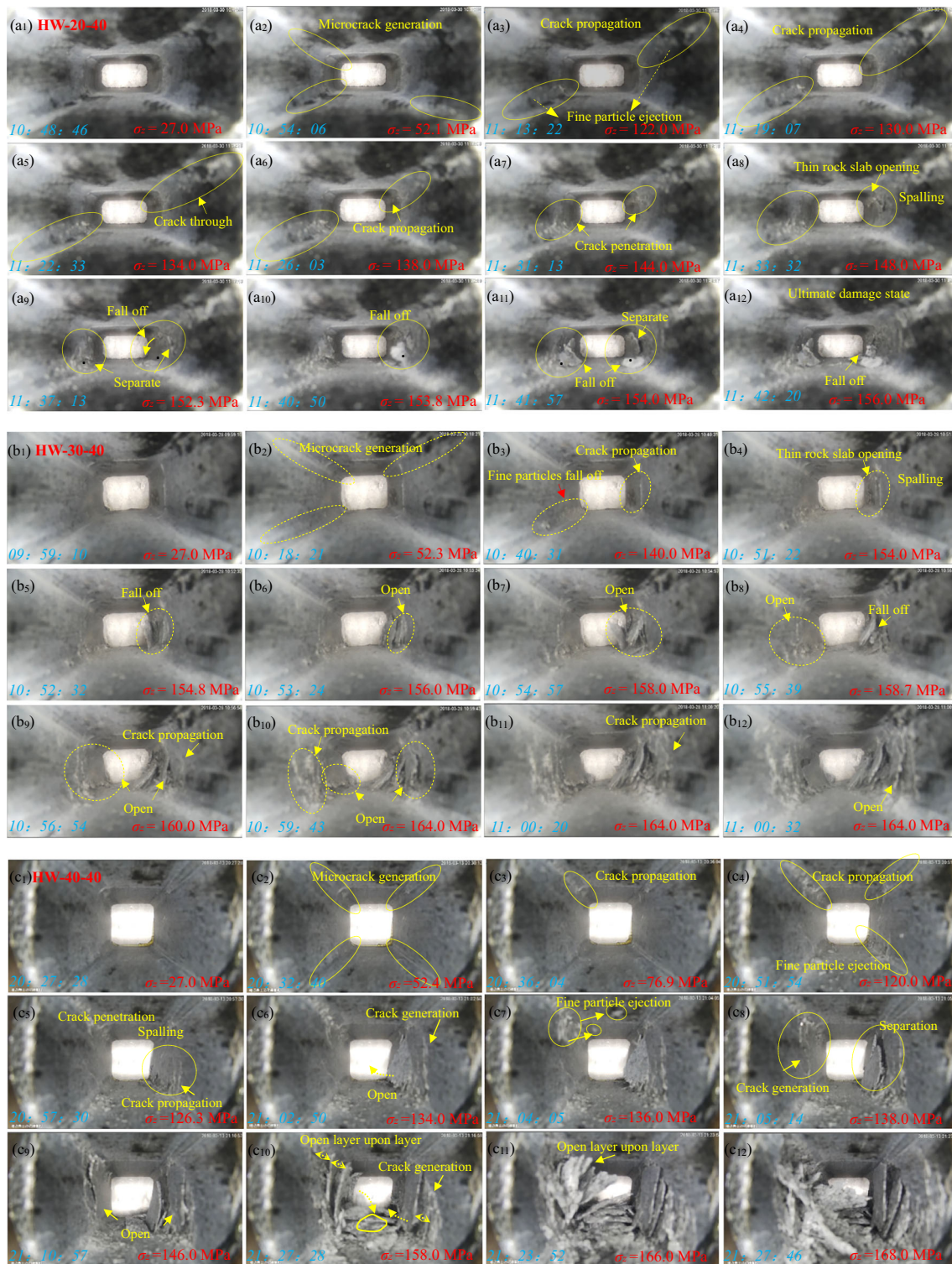


Fig. 9 Screenshots of specimen spalling process: **a** HW-20-40; **b** HW-30-40; **c** HW-40-40; **d** HW-40-30; **e** HW-40-20

slabs on the right sidewall were separated (Fig. 9a₁₁). Finally, when $\sigma_z = 156.0$ MPa, the right thin rock slab completely fell off, and no obvious damage on both sidewalls was observed until the end of the test (Fig. 9a₁₂).

Influence of different H/Ws on spalling failure

The vertical stress (σ_z) of each specimen at the initial failure is shown in Fig. 10, which shows that when the widths of the

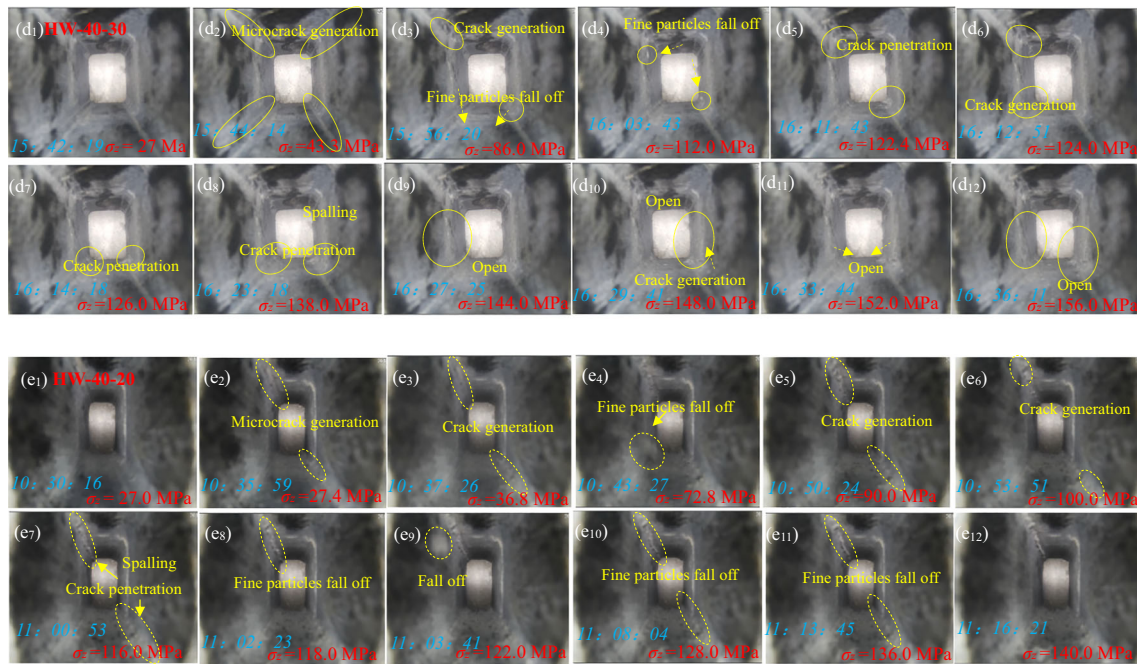


Fig. 9 (continued)

specimen were the same, σ_z required for the initial failure of the specimen was not much different as the height increased. Meanwhile, when the height was consistent, σ_z required for the initial failure of specimens significantly decreased with the decrease in the width. These results indicated that initial failure of the specimens is more likely to occur with the increase in H/W. Therefore, to analyse the influence of different H/Ws on the spalling-failure characteristics and stability of hard-rock rectangular tunnels, detailed analysis and discussion were carried out.

Figure 11 shows a comparison of the different heights of rectangular tunnels for the same width. When $\sigma_z = 150.0$ MPa,

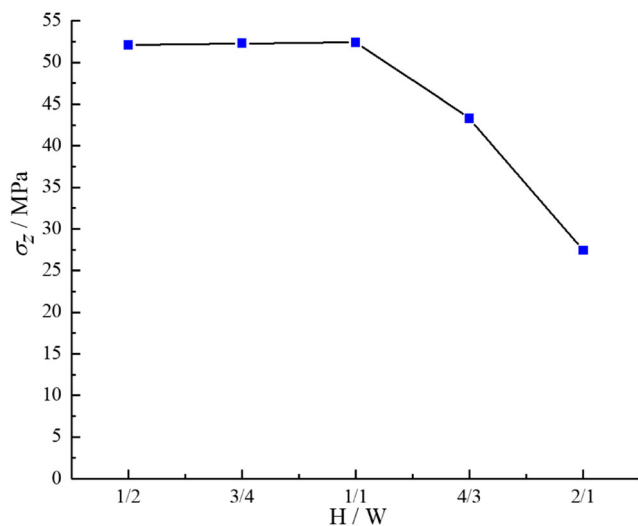


Fig. 10 Initial vertical stress magnitude in spalling failure

the sidewalls of HW-20-40 were destroyed. In particular, the thin rock slab on the right sidewall was opened (Fig. 11a₁). Meanwhile, those of HW-30-40 only exhibited fine particles falling off at the lower shoulder angle on the left sidewall, whereas the whole specimen remained intact (Fig. 11b₁). However, both sidewalls of the HW-40-40 exhibited obvious thin rock-slab opening (see Fig. 11c₁). With the increase in σ_z to 156.0 MPa, obvious thin rock-slab shedding phenomena appeared on both sidewalls of HW-20-40 (Fig. 11a₂). The thin rock slab on the right sidewall of HW-30-40 fell off, and the left sidewall remained intact (Fig. 11b₂). The damage degree of the HW-40-40 sidewall was obviously more serious than that of the other two specimens, the new thin rock slabs on the left sidewall continued to fall off, and the failure zone became larger (Fig. 11c₂). By combining Figs. 11 and 9a–c, a comparison of the rectangular-hole specimens at three different heights showed that the degree of damage of the rectangular holes from high to low followed the specimen order HW-40-40, HW-20-40, and HW-30-40. The spalling-failure degree did not decrease with the increase in the height.

Figure 12 shows the comparison of different widths of rectangular tunnels at the same height. When $\sigma_z = 134.0$ MPa, the thin rock slabs on the right sidewalls of HW-40-40 obviously opened (Fig. 12a₁). Cracks penetrated the upper left shoulder and lower right shoulder angles of HW-40-30, and bulges appeared on both sidewalls (Fig. 12b₁). Cracks penetrated the upper left shoulder and lower right shoulder angles of HW-40-20, but both sidewalls were not damaged (Fig. 12c₁). With the increase in σ_z to 140.0 MPa, the thin rock slab on the right sidewall of HW-40-40 further

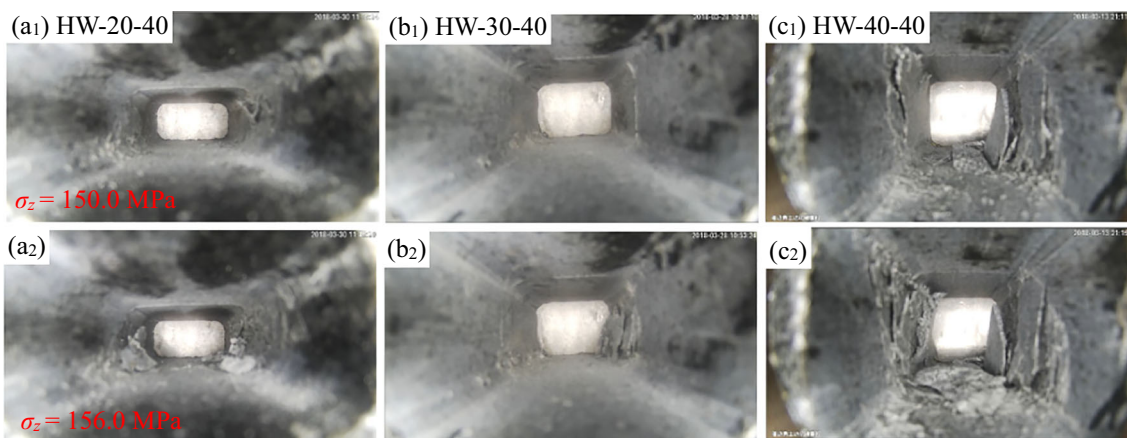


Fig. 11 Contrast chart of spalling failure degree of section shape with same width and different height under the same vertical stress: **a** HW-20-40; **b** HW-30-40; **c** HW-40-40

opened, whereas the crack penetration on the left sidewall led to opening of the thin rock slab (Fig. 12a₂). In contrast, both sidewalls of the HW-40-30 further bulged, and the damage at the shoulder angles on both sidewalls was more obvious (Fig. 12b₂). Conversely, at the shoulder angles on both sidewalls of the HW-40-20, the crack continued to propagate and penetrate in which fine particles fell off but the sidewall remained intact (Fig. 12c₂). By combining Fig. 12 and Figs. 9a–c, comparison of the rectangular-hole specimens at three different widths revealed that the degree of damage of the rectangular holes from high to low follow the following order: HW-40-40, HW-40-30 and HW-40-20. The spalling failure degree decreased with the decrease in the width.

Figures 13 and 14 show comparisons of different H/Ws for the same rectangular-section area. Figure 13 shows that under the same vertical stress, when the H/Ws were 1/2 (Fig. 13a₁) and 2/1 (Fig. 13 b₁), the stress concentration at the shoulder angle on both sidewalls was very obvious, which led to the continuous propagation and penetration of cracks at the shoulder angle and formation of an obvious failure zone. However, when the H/W was 1/2, obvious damage was observed on the

sidewall of the specimen, which released part of the energy (Fig. 13a₂). In contrast, when H/W was 2/1, the specimen was damaged only at the shoulder angle, but the sidewall remained intact (Fig. 13b₂). Further, cracks that propagated from the shoulder angle to the surface in HW-40-20 were observed, as shown in Fig. 7e, and obvious shear cracks were formed, which presented a greater risk of overall shear failure of the specimen. In summary, the spalling failure degree of the 2/1 H/W was lower than that of the 1/2 H/W, which could effectively restrain the development of spalling. Figure 14 shows that when $\sigma_z = 154.0$ MPa, thin rock-slab openings appeared on the sidewalls of both specimens (Figs. 14a₁ and b₁), but the thin rock-slab openings were more obvious in HW-30-40. When σ_z was increased to 156.0 MPa, the thin rock slabs formed on the right sidewall of HW-30-40 were detached, and new thin rock slabs were opened (Fig. 14a₂). In contrast, cracks on the sidewalls of HW-40-30 continued to develop and penetrated, and no obvious phenomenon of thin rock-slab opening was observed. Both sidewalls of the specimens were basically intact (Fig. 14b₂). Obviously, the spalling-failure degree of the 4/3 H/W was lower than that of the 3/4

Fig. 12 Contrast chart of spalling failure degree of section shape with same height and different width under the same vertical stress: **a** HW-40-40; **b** HW-40-30; **c** HW-40-20

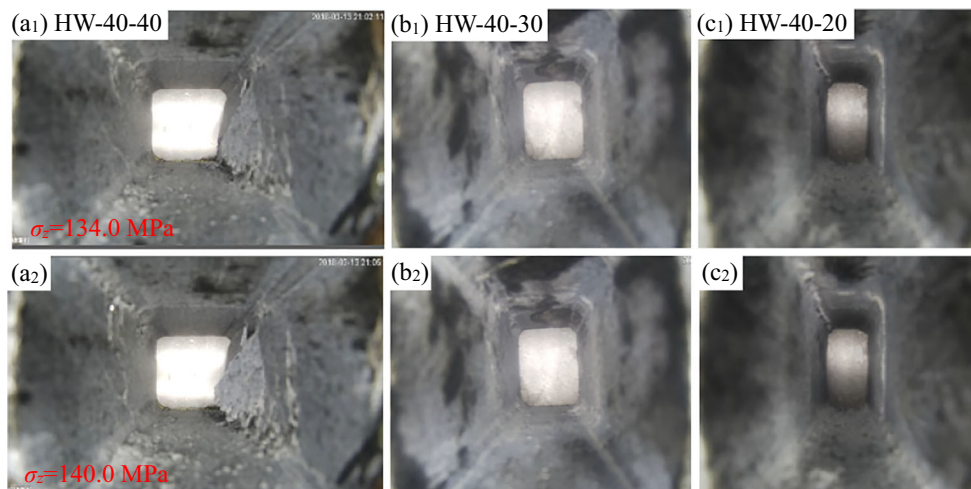
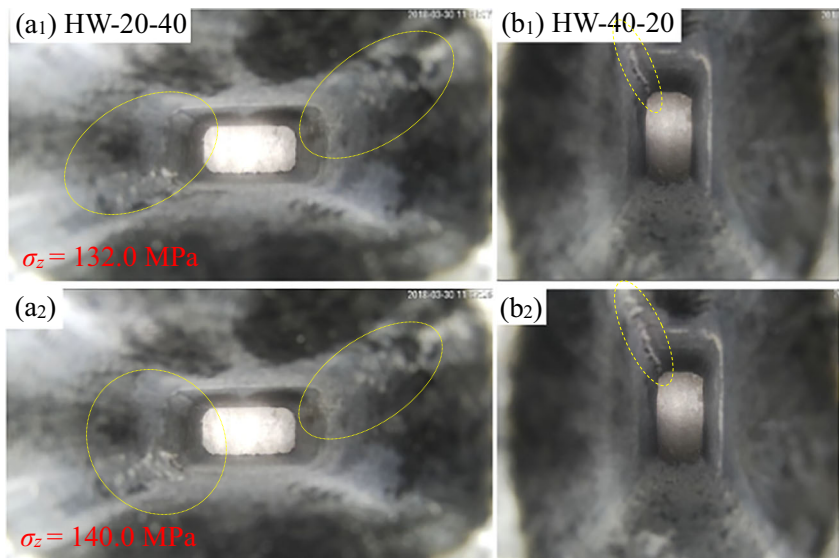


Fig. 13 The same cross-section area under the same vertical stress: **a** HW-20-40; **b** HW-40-20



H/W, which could effectively restrain the development of spalling. In summary, we can conclude that when the rectangular cross-sectional areas are the same, the arrangement in which the height is more than the width is adopted, which can improve the stability of the surrounding rocks of a tunnel and effectively reduce the degree of spalling.

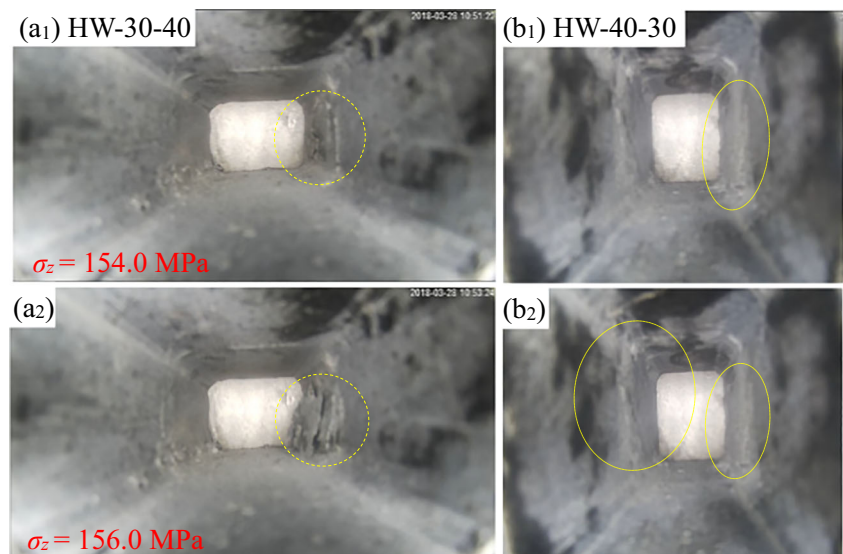
Conclusions

In this study, simulation tests of the spalling failure of a granite rectangular hole with different H/Ws were carried out, to determine the influence of the H/W of specimens on spalling failure. During the entire test process, the spalling failure in the rectangular holes was successfully reproduced by adjusting the vertical principal stress to the maximum

principal stress. The test results were analysed in detail, and the following conclusions were drawn.

- (1) Spalling process of the sidewall: a crack was first created at the shoulder angle of the sidewall in the rectangular hole and propagated along the axis. After the crack spread to a certain extent, spalling occurred in a local area on the sidewall. With the increase in stress, the crack continued to develop and penetrate, and the spalling failure gradually developed from the local area to the entire sidewall along the axial direction. The thin rock slabs continuously fell off.
- (2) Influence of the different H/Ws in the rectangular holes on the spalling failure. (a) When the rectangular-hole widths were the same, the spalling-failure degree did not decrease with the increase in the height. (b) When the heights of the rectangular holes

Fig. 14 The same cross-section area under the same vertical stress: **a** HW-30-40; **b** HW-40-30



were the same, the spalling failure degree decreased with the decrease in the width. (c) When the cross-sectional areas of the rectangular hole were the same, the arrangement in which the height was more than the width could effectively reduce the degree of spalling failure. (d) The larger the H/W of the rectangular hole, the more likely the stress concentrated at the shoulder angle of the sidewall, resulting in obvious crack propagation and penetration at the shoulder angle, which is prone to overall shear failure. (e) When the H/W of the rectangular hole was 1/1, the degree of spalling failure was the highest, which presented the greatest risk.

The aforementioned conclusions provide a theoretical basis for the selection and safety management of the sectional size of deeply buried rectangular tunnels. For safety management of rectangular tunnels with different H/Ws, crack monitoring at the shoulder angle of the sidewall should be emphasised, and supporting measures such as providing bolts on the sidewalls should be applied to improve the stability of the surrounding rock. As far as possible, the arrangement in which the height is more than the width can effectively reduce the degree of spalling failure.

Acknowledgements Many thanks to Jifu Gao, the general manager of JingCheng Geotechnical Service Company that locates in Liuyang City, Hunan Province of China, for his sincere help in processing rock specimens.

Funding information This work was supported by the National Natural Science Foundation of China (Grant No. 41472269), the Opening Fund of State Key Laboratory of Geohazard Prevention and Geoenvironment Protection (Chengdu University of Technology) (Grant No. SKLGP2018K010), and the Fundamental Research Funds for the Central Universities of Central South University (Grant No. 2019zzts673).

References

- Cai M, Kaiser PK (2018) Rockburst support reference book-volume I: Rockburst phenomenon and support characteristics. Mining Innovation, Laurentian University, Sudbury, Ontario
- Carter BJ (1992) Size and stress gradients effects on fracture around cavities. *Rock Mech Rock Eng* 25(3):167–186
- Cristescu ND, Paraschiv I (1995) The optimal shape of rectangular-like caverns. *Int J Rock Mech Min Sci Geomech Abstr* 32(4):285–300
- Du K, Tao M, Li XB, Zhou J (2016) Experimental study of slabbing and rockburst induced by true-triaxial unloading and local dynamic disturbance. *Rock Mech Rock Eng* 49(9):3437–3453
- Du K, Su R, Tao M, Yang CZ, Momen A, Wang SF (2019) Specimen shape and cross-section effects on the mechanical properties of rocks under uniaxial compressive stress. *Bull Eng Geol Environ*. <https://doi.org/10.1007/s10064-019-01518-x>
- Exadaktylos GE, Tsoutrelis CE (1995) Pillar failure by axial splitting in brittle rocks. *Int J Rock Mech Min Sci Geomech Abstr* 32(6):551–562
- Gong QM, Yin LJ, Wu SY, Zhao J, Ting Y (2012) Rock burst and slabbing failure and its influence on tbm excavation at headrace tunnels in Jinping II hydropower station. *Eng Geol* 124:98–108
- Gong FQ, Luo Y, Li XB, Si XF, Tao M (2018a) Experimental simulation investigation on rockburst induced by spalling failure in deep circular tunnels. *Tunn Undergr Space Technol* 81:413–427
- Gong FQ, Si XF, Li XB, Wang SY (2018b) Experimental investigation of strain rockburst in circular caverns under deep three-dimensional high stress conditions. *Rock Mech Rock Eng* 52(5):1459–1474
- Gong FQ, Wu WX, Li TB, Si XF (2019a) Simulation experimental study on spalling failure of surrounding rock in rectangular tunnel of deep hard rock. *Rock Soil Mech* 40(06):2085–2097 (in Chinese)
- Gong FQ, Wu C, Luo S, Yan JY (2019b) Load–unload response ratio characteristics of rock materials and their application in prediction of rockburst proneness. *Bull Eng Geol Environ* 78(7):5445–5466
- Gong FQ, Yan JY, Li XB, Luo S (2019c) A peak-strength strain energy storage index for rock burst proneness of rock materials. *Int J Rock Mech Min Sci* 117:76–89
- He MC, Miao JL, Feng JL (2010) Rock burst process of limestone and its acoustic emission characteristics under true-triaxial unloading conditions. *Int J Rock Mech Min Sci* 47(2):286–298
- He MC, Xia HM, Jia XN, Gong WL, Zhao F, Liang KY (2012) Studies on classification, criteria and control of rockbursts. *J Rock Mech Geotech Eng* 4(2):97–114
- He MC, Liu DQ, Gong WL, Wang CC, Kong J, Du S, Zhang S (2014) Development of a testing system for impact rockbursts. *Chin J Rock Mech Eng* 39(9):1729–1739 (in Chinese)
- Hoek E (1965) Rock fracture under static stress conditions. CSIR report MEG 383. National Mechanical Engineering Research Institute, Council for Scientific and Industrial Research, Pretoria
- Hoek E, Brown ET (2018) The Hoek-Brown failure criterion and GSI - 2018 edition. *J Rock Mech Geotech Eng* 11 (3), 445–463
- Hoek E, Kaiser PK, Bawden WF (1995) Support of underground excavations in hard rock. A.A. Balkema, Rotterdam, pp. 122–123
- Hou ZS, Gong QM, Jiao WG, Sun ZH (2013) Demonstration of concave deformation of arc-shaped rock slabs in deep circular tunnels. *Chi J Rock Mech Geo Eng* 35(3):551–558 (in Chinese)
- Jiang Q, Feng XT, Fan YL, Fan QX, Liu GF, Pei SF (2017) In situ experimental investigation of basalt spalling in a large underground powerhouse cavern. *Tunn Undergr Space Technol* 68:82–94
- Li SJ, Feng XT, Li ZH, Zhang CQ, Chen BR (2012) Evolution of fractures in the excavation damaged zone of a deeply buried tunnel during TBM construction. *Int J Rock Mech Min Sci* 55:125–138
- Li XB, Feng F, Li DY, Du K, Ranjith PG, Rostami J (2018a) Failure characteristics of granite influenced by specimen height-to-width ratios and intermediate principal stress under true-triaxial unloading conditions. *Rock Mech Rock Eng* 51(3):1–25
- Li XJ, He MC, Sun YB, Zhou RX, Wang L (2018b) Study on the splitting failure of the surrounding rock of underground caverns. *Geomech Eng* 14(5):10–27
- Liang CY, Zhang QB, Li X, Xin P (2016) The effect of specimen shape and strain rate on uniaxial compressive behavior of rock material. *Bull Eng Geol Environ* 75(4):1669–1681
- Martin CD (1993) Strength of massive Lac du Bonnet granite around underground openings. Ph.D. thesis, Department of Civil and Geological Engineering, University of Manitoba, Winnipeg, Man
- Martin CD (1997) Seventeenth Canadian geotechnical colloquium: the effect of cohesion loss and stress path on brittle rock strength. *Can Geotech J* 34(5):698–725
- Martin CD, Read RS, Martino JB (1997) Observations of brittle failure around a circular test tunnel. *Int J Rock Mech Min Sci Geomech Abstr* 34(7):1065–1073
- Ren G, Smith JV, Tang JW, Xie YM (2005) Underground excavation shape optimization using an evolutionary procedure. *Comput Geotech* 32(2):122–132

- Stacey TR (1981) A simple extension strain criterion for fracture of brittle rock. *Int J Rock Mech Min Sci Geomech Abstr* 18(6):469–474
- Su GS, Jiang JQ, Feng XT, Jiang Q, Chen ZY, Mo JH (2019) Influence of loading rate on strainburst: an experimental study. *Bull Eng Geol Environ* 78(5):3559–3573
- Tuncay E, Hasancebi N (2009) The effect of length to diameter ratio of test specimens on the uniaxial compressive strength of rock. *Bull Eng Geol Environ* 68(4):491–497
- Xu NW, Li TB, Dai F, Zhang R, Tang CA, Tang XL (2016) Microseismic monitoring of strainburst activities in deep tunnels at the Jinping II hydropower station, China. *Rock Mech Rock Eng* 49(3):981–1000
- Zhao F, He MC (2016) Size effects on granite behavior under unloading rockburst test. *Bull Eng Geol Environ* 76(3):1183–1197
- Zhou H, Lu JJ, Hu SC, Zhang CQ, Xu RC, Meng FZ (2016) Influence of curvature radius of tunnels excavation section on slabbing of hard brittle rockmass under high stress. *Rock Soil Mech* 31(1):140–146 (in Chinese)
- Zhu WS, Yang WM, Li XJ, Xiang L, Yu DJ (2014) Study on splitting failure in rock masses by simulation test, site monitoring and energy model. *Tunn Undergr Space Technol* 41:152–164